Comput Mech (2013) 51:899–909
DOI 10.1007/s00466-012-0769-8

ORIGINAL PAPER

A simplified implementation of a gradient-enhanced damage model with transient length scale effects

S. Saroukhani · R. Vafadari · A. Simone

Received: 21 February 2012 / Accepted: 17 July 2012 / Published online: 1 August 2012

Abstract Gradient-enhanced damage models with constant gradient activity suffer from spurious damage growth at high deformation levels. This issue was resolved by Geers et al. (Comput Methods Appl Mech Eng 160(1–2):133–153, 1998) by expressing the gradient activity parameter as a function of the local equivalent strain at the expense of adding one set of degrees of freedom to those of the standard model. In this contribution, a new formulation of the gradient-enhanced damage model with variable length scale is presented which eliminates the need for the extra set of degrees of freedom. The merits of the proposed formulation are demonstrated, and the choice of the damage evolution law and its impact on the model performance are discussed.

Keywords Continuum damage mechanics · Regularized media · Gradient-enhanced damage models · Transient internal length scale

1 Introduction

Failure in quasi-brittle materials stems from the nucleation and accumulation of micro-cracks and culminates with the formation and propagation of traction-free macro-cracks. A sound computational framework for modeling such a phenomenon should provide a realistic description of these processes.

Numerous computational techniques are now available for tracing the events that take place during failure. With reference to continuum damage models, nonlocal approaches [3,4,18] are among the most successful. In these models, the quantity driving damage evolution at a material point is computed as a weighted average of a measure of local deformation at the surrounding points. The weight function of the averaging process is directly related to an internal length scale which controls how a material point is affected by the behavior of surrounding points. Initial versions of these methods adopted a constant internal length scale which resulted in spurious damage growth in inactive regions at high deformation levels [19]. This is attributed [8] to the fact that the nonlocal averaging process remains active at all material points through the entire load history and, as a result, highly localized strains within the process zone are mapped to surrounding points.

Although limited experimental knowledge is available regarding the evolution of the internal length scale, micromechanical arguments have shown that the interaction between cracks and voids is of a transient nature in the course of failure [1,2]. Pijaudier-Cabot et al. [19] made use of this argument to introduce a nonlocal model with evolving length scale, whereby the internal length is made a function of local damage expressed in terms of the local equivalent strain. Compared to the original nonlocal damage model, the model with evolving length scale delivers physically acceptable damage profiles at high deformation levels. More recently, other nonlocal damage models with evolving length scale have been proposed [6,7,9,15]. In particular, the stress-based model by Giry et al. [9] is very effective in solving the issues discussed by Simone et al. [21] in terms of damage initiation and propagation. In this context, it is worth mentioning that also gradient plasticity models can benefit from the use of an evolving length scale as demonstrated by Voyiadjis and Abu Al-Rub [22].

The implicit gradient-enhanced damage model proposed by Peerlings et al. [17] can be considered as an approximated differential version of the nonlocal damage model pro-

S. Saroukhani · R. Vafadari · A. Simone (✉)
Faculty of Civil Engineering and Geosciences, Delft University of Technology, P.O. Box 5048, 2600 GA Delft, The Netherlands
e-mail: a.simone@tudelft.nl

posed by Pijaudier-Cabot and Bažant [18]. In this model, the gradient activity parameter is the counterpart of the internal length scale parameter. Similar to the original nonlocal damage model [18], the implicit gradient-enhanced damage model adopts a constant length scale and fails to deliver physically acceptable damage profiles at high deformation levels [21].

The concept of an evolving length scale appeared in gradient models sooner than their nonlocal counterparts. Geers et al. [8] proposed an implicit gradient-enhanced damage model with a transient gradient activity parameter expressed as a function of the local equivalent strain. This approach eliminates the spurious damage growth associated with the method with constant gradient activity [17]. However, the model involves an extra continuity equation on either the gradient activity parameter or the local equivalent strain and therefore adds a set of degrees of freedom to those of the standard model.

In this contribution, a new formulation of the implicit gradient-enhanced damage model with transient length scale is presented which eliminates the need for the extra set of degrees of freedom from the model developed by Geers et al. [8]. In the following section, the original implicit gradient-enhanced damage model is briefly described and an explanation for the necessity of the extra set of degrees of freedom is provided. Section 3 entails the derivations of the weak form of the new formulation. In Sect. 4, the weak form of the governing equations is discretized and the corresponding consistent incremental-iterative scheme is presented. Finally, in Sect. 5, the merits of the method are demonstrated by one- and two-dimensional examples.

2 Implicit gradient-enhanced damage model with constant and transient gradient activity

The gradient-enhanced damage model by Peerlings et al. [17] is described by a system of coupled differential equations expressed in terms of the classical equilibrium equation

$$\boldsymbol{\nabla}\cdot\boldsymbol{\sigma}+\boldsymbol{b}=\boldsymbol{0} \quad \text{in} \quad \Omega \tag{1}$$

and the modified Helmholtz equation (diffusion equation)

$$\bar{e}-c\nabla^2\bar{e}=e \quad \text{in} \quad \Omega, \tag{2}$$

completed by the standard boundary conditions for the equilibrium equations and by

$$\boldsymbol{\nabla}\bar{e}\cdot\boldsymbol{n}=0 \quad \text{on} \quad \Gamma \tag{3}$$

for the diffusion equation.In the above equations, $\boldsymbol{\sigma}$ is the stress tensor, $\boldsymbol{b}$ the vector of body forces, $\bar{e}$ is the nonlocal equivalent strain, c is the constant gradient activity parameter, e is the local equivalent strain defined as a scalar measure of the strain tensor $\boldsymbol{\varepsilon}$, and $\boldsymbol{n}$ is the outward unit normal vector on the boundary Γ of the body Ω.Stress and strain tensors are related through

$$\boldsymbol{\sigma}=(1-\omega)\,\boldsymbol{C}:\boldsymbol{\varepsilon}, \tag{4}$$

where $\boldsymbol{C}$ is the fourth order tensor of elastic moduli and the scalar damage variable ω varies between 0 and 1, indicating undamaged and completely damaged material, respectively. Damage is driven by the most severe deformation, expressed through a scalar history parameter κ, reached at a material point. The history parameter is governed by the usual Kuhn-Tucker relations which are expressed in terms of the nonlocal equivalent strain [17].

In the original formulation of the gradient-enhanced damage models (1)–(4), the gradient activity parameter c is considered to be constant and equal to $1/2l^2$, where l is the length scale parameter. The consequences of this choice have been discussed by Geers et al. [8]. They showed that the constant gradient-enhanced damage (CGD) model fails to render physically acceptable results for situations characterized by considerable deformation levels. In such cases, the weighting function related to the diffusion equation (2) maps the localized strain within the fracture zone to the nonlocal equivalent strain related to neighboring material points. Consequently, spurious damage growth can be observed around highly damaged zones and in regions that should only unload.To address this problem, Geers et al. [8] proposed a strain-based transient-gradient damage (STGD) model whereby the nonlocal interaction is controlled by the transient gradient activity parameter

$$\xi(e)=\begin{cases} c\left(\frac{e}{e_\xi}\right)^{n_\xi} & \text{if} \quad e\le e_\xi \\ c & \text{if} \quad e>e_\xi \end{cases}, \tag{5}$$

where e_ξ and n_ξ are model parameters. The above expression implies that nonlocal coupling starts as soon as deformation is detected at a material point and reaches its maximum level, namely c, when the local equivalent strain is e_ξ. The consequences of this choice are twofold. On the one hand, nonlocal interaction is progressively mobilized as the local equivalent strain increases. On the other hand, at considerable deformation levels, ξ vanishes in the unloaded material surrounding the process zone. Hence, nonlocal interaction is appropriately confined and the unloaded material behaves in a local manner.

However, when a transient gradient activity parameter ξ is considered in (2) according to

$$\bar{e}-\xi\nabla^2\bar{e}=e, \tag{6}$$

the coupled set of governing equations (1) and (6) needs to be augmented with a continuity equation on ξ [8]. This is related to the presence of the gradient of ξ in the weak formulation of equation (6) and results in an additional degree of freedom per node. In this contribution, a simplified implementation

of the strain-based transient-gradient damage model is presented which retains the same features as the model by Geers et al. [8] with the advantage of requiring the same number of degrees of freedom as the gradient-enhanced damage model by Peerlings et al. [17].

3 A modified strain-based transient-gradient damage model

To circumvent the need for an extra continuity equation, it is sufficient to divide (6) by $\xi \neq 0$. This yields the diffusion equation

$$\frac{\bar{e}}{\xi} - \nabla^2 \bar{e} = \frac{e}{\xi}. \tag{7}$$

The weighted residual approach is used to obtain the weak format of the governing equations. To this end, (1) and (7) are multiplied by the vectorial function $\boldsymbol{w}_\mathrm{u}$ and the scalar function w_e, respectively. The resulting equations are then integrated over Ω to yield

$$\int_\Omega \boldsymbol{w}_\mathrm{u} \cdot (\nabla \cdot \boldsymbol{\sigma} + \boldsymbol{b}) \, \mathrm{d}\Omega = 0 \quad \forall \ \boldsymbol{w}_\mathrm{u} \in H_0^1(\Omega) \tag{8}$$

and

$$\int_\Omega w_\mathrm{e} \left(\frac{\bar{e}}{\xi} - \nabla^2 \bar{e} \right) \mathrm{d}\Omega = \int_\Omega w_\mathrm{e} \frac{e}{\xi} \, \mathrm{d}\Omega \quad \forall \ w_\mathrm{e} \in H^1(\Omega). \tag{9}$$

Next, the identities

$$\boldsymbol{w}_\mathrm{u} \cdot (\nabla \cdot \boldsymbol{\sigma}) = \nabla \cdot (\boldsymbol{w}_\mathrm{u} \cdot \boldsymbol{\sigma}) - (\nabla \boldsymbol{w}_\mathrm{u}) : \boldsymbol{\sigma} \tag{10}$$

and

$$w_\mathrm{e} \nabla^2 \bar{e} = \nabla \cdot (w_\mathrm{e} \cdot \nabla \bar{e}) - \nabla w_\mathrm{e} \cdot \nabla \bar{e} \tag{11}$$

are substituted in (8) and (9). This leads to

$$\int_\Omega [\nabla \boldsymbol{w}_\mathrm{u} : \boldsymbol{\sigma} - \boldsymbol{w}_\mathrm{u} \cdot \boldsymbol{b} - \nabla \cdot (\boldsymbol{w}_\mathrm{u} \cdot \boldsymbol{\sigma})] \, \mathrm{d}\Omega = 0 \tag{12}$$

and

$$\int_\Omega \left[w_\mathrm{e} \frac{\bar{e}}{\xi} - \nabla \cdot (w_\mathrm{e} \cdot \nabla \bar{e}) + \nabla w_\mathrm{e} \cdot \nabla \bar{e} \right] \mathrm{d}\Omega = \int_\Omega w_\mathrm{e} \frac{e}{\xi} \, \mathrm{d}\Omega. \tag{13}$$

The weak form of the governing equations of the modified strain-based transient-gradient damage model is obtained using the divergence theorem and applying the boundary conditions $\boldsymbol{\sigma} \cdot \boldsymbol{n} = \boldsymbol{p}$ and $\nabla \bar{e} \cdot \boldsymbol{n} = 0$ on Γ:

$$\int_\Omega \nabla \boldsymbol{w}_\mathrm{u} : \boldsymbol{\sigma} \, \mathrm{d}\Omega = \int_\Omega \boldsymbol{w}_\mathrm{u} \cdot \boldsymbol{b} \, \mathrm{d}\Omega + \int_\Gamma \boldsymbol{w}_\mathrm{u} \cdot \boldsymbol{p} \, \mathrm{d}\Gamma, \tag{14}$$

$$\int_\Omega \left(w_\mathrm{e} \frac{\bar{e}}{\xi} + \nabla w_\mathrm{e} \cdot \nabla \bar{e} \right) \mathrm{d}\Omega = \int_\Omega w_\mathrm{e} \frac{e}{\xi} \, \mathrm{d}\Omega. \tag{15}$$

As it is obvious from (15), the gradient of ξ is no longer involved in the weak form of the diffusion equation. Unlike the strain-based transient-gradient damage model by Geers et al. [8], an extra continuity equation is not necessary.

4 Finite element formulation

4.1 Discretization

The Bubnov-Galerkin method is employed for the discretization of the weak form of the governing equations. To this end, the displacement and the nonlocal equivalent strain fields, along with the corresponding weight functions, are discretized at the element level as follows:

$$\begin{aligned} &\boldsymbol{u}^\mathrm{h} = \boldsymbol{N}_\mathrm{u} \boldsymbol{u}, \quad \boldsymbol{w}_\mathrm{u}^\mathrm{h} = \boldsymbol{N}_\mathrm{u} \boldsymbol{w}_\mathrm{u}, \quad \bar{e}^\mathrm{h} = \boldsymbol{N}_\mathrm{e} \bar{\boldsymbol{e}}, \quad w_\mathrm{e}^\mathrm{h} = \boldsymbol{N}_\mathrm{e} \boldsymbol{w}_\mathrm{e}, \\ &\nabla \bar{e}^\mathrm{h} = \boldsymbol{B}_\mathrm{e} \bar{\boldsymbol{e}}, \quad \nabla w_\mathrm{e}^\mathrm{h} = \boldsymbol{B}_\mathrm{e} \boldsymbol{w}_\mathrm{e}, \quad \nabla \boldsymbol{w}_\mathrm{u}^\mathrm{h} = \boldsymbol{B}_\mathrm{u} \boldsymbol{w}_\mathrm{u}, \end{aligned} \tag{16}$$

where the shape function matrices $\boldsymbol{N}_\mathrm{u}$ and $\boldsymbol{N}_\mathrm{e}$ interpolate the nodal values $\boldsymbol{u}$ and $\bar{\boldsymbol{e}}$, respectively, and $\boldsymbol{B}_\mathrm{u}$ and $\boldsymbol{B}_\mathrm{e}$ are the gradient operators for the displacement and the nonlocal equivalent strain, respectively. The same shape functions are used to interpolate the nodal values of the weight functions $\boldsymbol{w}_\mathrm{u}$ and $\boldsymbol{w}_\mathrm{e}$. Inserting relations (16) into the weak formulation of the governing equations and expressing the stress and strain tensors in their vector form yield

$$\int_\Omega \boldsymbol{w}_\mathrm{u}^\mathrm{T} \boldsymbol{B}_\mathrm{u}^\mathrm{T} \boldsymbol{\sigma} \, \mathrm{d}\Omega = \int_\Omega \boldsymbol{w}_\mathrm{u}^\mathrm{T} \boldsymbol{N}_\mathrm{u}^\mathrm{T} \boldsymbol{b} \, \mathrm{d}\Omega + \int_\Gamma \boldsymbol{w}_\mathrm{u}^\mathrm{T} \boldsymbol{N}_\mathrm{u}^\mathrm{T} \boldsymbol{p} \, \mathrm{d}\Gamma \tag{17}$$

and

$$\int_\Omega \boldsymbol{w}_\mathrm{e}^\mathrm{T} \left(\boldsymbol{N}_\mathrm{e}^\mathrm{T} \boldsymbol{N}_\mathrm{e} \frac{\bar{\boldsymbol{e}}}{\xi} + \boldsymbol{B}_\mathrm{e}^\mathrm{T} \boldsymbol{B}_\mathrm{e} \bar{\boldsymbol{e}} \right) \mathrm{d}\Omega = \int_\Omega \boldsymbol{w}_\mathrm{e}^\mathrm{T} \boldsymbol{N}_\mathrm{e}^\mathrm{T} \frac{e}{\xi} \, \mathrm{d}\Omega, \tag{18}$$

which have to hold for any choice of $\boldsymbol{w}_\mathrm{u}$ and $\boldsymbol{w}_\mathrm{e}$. Therefore, the final discretized expression of the governing equations is:

$$\int_\Omega \boldsymbol{B}_\mathrm{u}^\mathrm{T} \boldsymbol{\sigma} \, \mathrm{d}\Omega = \int_\Omega \boldsymbol{N}_\mathrm{u}^\mathrm{T} \boldsymbol{b} \, \mathrm{d}\Omega + \int_\Gamma \boldsymbol{N}_\mathrm{u}^\mathrm{T} \boldsymbol{p} \, \mathrm{d}\Gamma, \ \text{and} \tag{19}$$

$$\int_\Omega \left(\boldsymbol{N}_\mathrm{e}^\mathrm{T} \boldsymbol{N}_\mathrm{e} \frac{\bar{\boldsymbol{e}}}{\xi} + \boldsymbol{B}_\mathrm{e}^\mathrm{T} \boldsymbol{B}_\mathrm{e} \bar{\boldsymbol{e}} \right) \mathrm{d}\Omega = \int_\Omega \boldsymbol{N}_\mathrm{e}^\mathrm{T} \frac{e}{\xi} \, \mathrm{d}\Omega. \tag{20}$$

Finally, the discretized governing equations are rewritten in terms of external and internal nodal forces according to

$$\boldsymbol{f}^{\mathrm{u}}_{\mathrm{int}} = \boldsymbol{f}^{\mathrm{u}}_{\mathrm{ext}} \quad \text{and} \quad \boldsymbol{f}^{\bar{\mathrm{e}}}_{\mathrm{int}} = \boldsymbol{f}^{\bar{\mathrm{e}}}_{\mathrm{ext}} \tag{21}$$

where

$$\boldsymbol{f}^{\mathrm{u}}_{\mathrm{int}} = \int_{\Omega} \boldsymbol{B}^{\mathrm{T}}_{\mathrm{u}} \boldsymbol{\sigma} \, \mathrm{d}\Omega, \tag{22}$$

$$\boldsymbol{f}^{\mathrm{u}}_{\mathrm{ext}} = \int_{\Omega} \boldsymbol{N}^{\mathrm{T}}_{\mathrm{u}} \boldsymbol{b} \, \mathrm{d}\Omega + \int_{\Gamma} \boldsymbol{N}^{\mathrm{T}}_{\mathrm{u}} \boldsymbol{p} \, \mathrm{d}\Gamma, \tag{23}$$

$$\boldsymbol{f}^{\bar{\mathrm{e}}}_{\mathrm{int}} = \int_{\Omega} \left(\boldsymbol{N}^{\mathrm{T}}_{\mathrm{e}} \boldsymbol{N}_{\mathrm{e}} \frac{\bar{\boldsymbol{e}}}{\xi} + \boldsymbol{B}^{\mathrm{T}}_{\mathrm{e}} \boldsymbol{B}_{\mathrm{e}} \bar{\boldsymbol{e}} \right) \mathrm{d}\Omega - \int_{\Omega} \boldsymbol{N}^{\mathrm{T}}_{\mathrm{e}} \frac{e}{\xi} \, \mathrm{d}\Omega, \tag{24}$$

$$\boldsymbol{f}^{\bar{\mathrm{e}}}_{\mathrm{ext}} = \boldsymbol{0}. \tag{25}$$

4.2 Consistent incremental-iterative scheme

A consistent tangent stiffness is obtained by linearizing (21) at iteration $i+1$ with respect to the previous iteration i. Accordingly,

$$\boldsymbol{f}^{\mathrm{u}}_{\mathrm{ext}} = \boldsymbol{f}^{\mathrm{u}}_{\mathrm{int},i} + \delta \boldsymbol{f}^{\mathrm{u}}_{\mathrm{int}} \tag{26}$$

and

$$\boldsymbol{f}^{\bar{\mathrm{e}}}_{\mathrm{ext}} = \boldsymbol{f}^{\bar{\mathrm{e}}}_{\mathrm{int},i} + \delta \boldsymbol{f}^{\bar{\mathrm{e}}}_{\mathrm{int}}, \tag{27}$$

where

$$\delta \boldsymbol{f}^{\mathrm{u}}_{\mathrm{int}} = \int_{\Omega} \boldsymbol{B}^{\mathrm{T}}_{\mathrm{u}} \delta \boldsymbol{\sigma} \, \mathrm{d}\Omega \tag{28}$$

and

$$\delta \boldsymbol{f}^{\bar{\mathrm{e}}}_{\mathrm{int}} = \int_{\Omega} \left(-\boldsymbol{N}^{\mathrm{T}}_{\mathrm{e}} \boldsymbol{N}_{\mathrm{e}} \frac{\delta \xi}{\xi^2} \bar{\boldsymbol{e}} + \boldsymbol{N}^{\mathrm{T}}_{\mathrm{e}} \frac{1}{\xi} \boldsymbol{N}_{\mathrm{e}} \delta \bar{\boldsymbol{e}} + \boldsymbol{B}^{\mathrm{T}}_{\mathrm{e}} \boldsymbol{B}_{\mathrm{e}} \delta \bar{\boldsymbol{e}} - \boldsymbol{N}^{\mathrm{T}}_{\mathrm{e}} \frac{\delta e}{\xi} + \boldsymbol{N}^{\mathrm{T}}_{\mathrm{e}} \frac{\delta \xi}{\xi^2} e \right) \mathrm{d}\Omega. \tag{29}$$

Variations $\delta \boldsymbol{\sigma}_{i+1}$ of the stress tensor are obtained considering (4):

$$\delta \boldsymbol{\sigma}_{i+1} = (1 - \omega_i) \, \boldsymbol{C} \delta \boldsymbol{\varepsilon}_{i+1} - \boldsymbol{C} \boldsymbol{\varepsilon}_i \delta \omega_{i+1}, \tag{30}$$

where

$$\delta \boldsymbol{\varepsilon}_{i+1} = \boldsymbol{B}_{\mathrm{u}} \delta \boldsymbol{u}_{i+1} \tag{31}$$

and

$$\delta \omega_{i+1} = \frac{\partial \omega}{\partial \kappa}\Big|_i \frac{\partial \kappa}{\partial \bar{e}}\Big|_i \delta \bar{e}_{i+1} = \frac{\partial \omega}{\partial \kappa}\Big|_i \frac{\partial \kappa}{\partial \bar{e}}\Big|_i \boldsymbol{N}_{\mathrm{e}} \delta \bar{\boldsymbol{e}}_{i+1}, \tag{32}$$

in which the relation $\delta \bar{e}_{i+1} = \boldsymbol{N}_{\mathrm{e}} \delta \bar{\boldsymbol{e}}_{i+1}$ has been used. The resulting stress variations are then inserted into (28) to obtain the iterative change of the internal nodal forces

$$\delta \boldsymbol{f}^{\mathrm{u}}_{\mathrm{int}} = \int_{\Omega} \boldsymbol{B}^{\mathrm{T}}_{\mathrm{u}} \left[(1 - \omega_i) \, \boldsymbol{C} \boldsymbol{B}_{\mathrm{u}} \delta \boldsymbol{u}_{i+1} - \boldsymbol{C} \boldsymbol{\varepsilon}_i \frac{\partial \omega}{\partial \kappa}\Big|_i \frac{\partial \kappa}{\partial \bar{e}}\Big|_i \boldsymbol{N}_{\mathrm{e}} \delta \bar{\boldsymbol{e}}_{i+1} \right] \mathrm{d}\Omega \tag{33}$$

which completes the linearization of the equilibrium equation (26).

The linearization of (29) requires the expression of variations $\delta \xi$ and δe. The gradient activity parameter ξ can be made a function of damage, local equivalent strain, or nonlocal equivalent strain. This implies that different expressions of its variation with respect to the nonlocal equivalent strain can be obtained. For instance, if ξ is assumed to be a function of damage then

$$\delta \xi_{i+1} = \frac{\partial \xi}{\partial \omega}\Big|_i \frac{\partial \omega}{\partial \kappa}\Big|_i \frac{\partial \kappa}{\partial \bar{e}}\Big|_i \boldsymbol{N}_{\mathrm{e}} \delta \bar{\boldsymbol{e}}_{i+1}. \tag{34}$$

However, micromechanical arguments and some experimental results show that the gradient activity parameter is an increasing function of the local equivalent strain [19]. This assumption, which is also used in this contribution, leads to vanishing variations of ξ with respect to the nonlocal equivalent strain,

$$\frac{\partial \xi}{\partial \bar{e}}\Big|_i = 0, \tag{35}$$

which in turn yield

$$\delta \xi_{i+1} = 0. \tag{36}$$

As for the variations of the local equivalent strain, they can be expressed as:

$$\delta e_{i+1} = \frac{\partial e}{\partial \boldsymbol{\varepsilon}}\Big|_i \delta \boldsymbol{\varepsilon}_{i+1} = \frac{\partial e}{\partial \boldsymbol{\varepsilon}}\Big|_i \boldsymbol{B}_{\mathrm{u}} \delta \boldsymbol{u}_{i+1}. \tag{37}$$

Variations $\delta \xi_{i+1}$ and δe_{i+1} can be inserted into (29) to yield

$$\delta \boldsymbol{f}^{\bar{\mathrm{e}}}_{\mathrm{int}} = \int_{\Omega} \left[\frac{1}{\xi}_i \left(\boldsymbol{N}^{\mathrm{T}}_{\mathrm{e}} \boldsymbol{N}_{\mathrm{e}} \delta \bar{\boldsymbol{e}}_{i+1} - \boldsymbol{N}^{\mathrm{T}}_{\mathrm{e}} \frac{\partial e}{\partial \boldsymbol{\varepsilon}}\Big|_i \boldsymbol{B}_{\mathrm{u}} \delta \boldsymbol{u}_{i+1} \right) + \boldsymbol{B}^{\mathrm{T}}_{\mathrm{e}} \boldsymbol{B}_{\mathrm{e}} \delta \bar{\boldsymbol{e}}_{i+1} \right] \mathrm{d}\Omega \tag{38}$$

which completes the linearization of the diffusion Eq. (27).

The linearized equilibrium and diffusion equations are then summarized in the following system of equations:

$$\begin{bmatrix} \boldsymbol{K}^{\mathrm{uu}}_i & \boldsymbol{K}^{\mathrm{ue}}_i \\ \boldsymbol{K}^{\mathrm{eu}}_i & \boldsymbol{K}^{\mathrm{ee}}_i \end{bmatrix} \begin{bmatrix} \delta \boldsymbol{u}_{i+1} \\ \delta \bar{\boldsymbol{e}}_{i+1} \end{bmatrix} = \begin{bmatrix} \boldsymbol{f}^{\mathrm{u}}_{\mathrm{ext}} \\ \boldsymbol{f}^{\bar{\mathrm{e}}}_{\mathrm{ext}} \end{bmatrix} - \begin{bmatrix} \boldsymbol{f}^{\mathrm{u}}_{\mathrm{int},i} \\ \boldsymbol{f}^{\bar{\mathrm{e}}}_{\mathrm{int},i} \end{bmatrix}, \tag{39}$$

Table 1 Parameters for the one-dimensional localization test

Geometry and model parameters	Quantity	Value	Units
Geometry	Length	100	mm
	Imperfection length	2.5	mm
	Cross-section	55	mm^2
	Cross-section (imperfection)	50	mm^2
Elastic parameters	Young's modulus E	4500	MPa
Nonlocal parameters	Gradient parameter c	5	mm^2
	n_ξ	1	–
	e_ξ	0.15 ($=10\kappa_\mathrm{i}$)	–
	c_0	0.01	–
Damage law	κ_i	0.015	–
	κ_c	0.5	–
	α	5	–
	β	0.8	–

where

$$\boldsymbol{K}_i^{\mathrm{uu}} = \int_\Omega \boldsymbol{B}_\mathrm{u}^\mathrm{T} (1-\omega_i)\, \boldsymbol{C}\boldsymbol{B}_\mathrm{u}\, \mathrm{d}\Omega, \tag{40}$$

$$\boldsymbol{K}_i^{\mathrm{ue}} = \int_\Omega -\boldsymbol{B}_\mathrm{u}^\mathrm{T} \boldsymbol{C}\boldsymbol{\varepsilon}_i \frac{\partial \omega}{\partial \kappa}\Big|_i \frac{\partial \kappa}{\partial \bar{e}}\Big|_i \boldsymbol{N}_\mathrm{e}\, \mathrm{d}\Omega, \tag{41}$$

$$\boldsymbol{K}_i^{\mathrm{eu}} = -\int_\Omega \boldsymbol{N}_\mathrm{e}^\mathrm{T} \frac{1}{\xi}_i \frac{\partial e}{\partial \boldsymbol{\varepsilon}}\Big|_i \boldsymbol{B}_\mathrm{u}\, \mathrm{d}\Omega, \tag{42}$$

$$\boldsymbol{K}_i^{\mathrm{ee}} = \int_\Omega \left(\boldsymbol{N}_\mathrm{e}^\mathrm{T} \frac{1}{\xi}_i \boldsymbol{N}_\mathrm{e} + \boldsymbol{B}_\mathrm{e}^\mathrm{T} \boldsymbol{B}_\mathrm{e} \right) \mathrm{d}\Omega. \tag{43}$$

The algorithmic treatment of this system of equations is identical to that of the CGD model [17]. From the implementation point of view, the introduction of a transient gradient activity parameter into a CGD model finite element code requires only trivial modifications. These modifications consist of dividing the integrands in the $\boldsymbol{K}^{\mathrm{eu}}$, $\boldsymbol{K}^{\mathrm{ee}}$, and $\delta \boldsymbol{f}_{\mathrm{int}}^{\bar{\mathrm{e}}}$ terms of the CGD model by ξ, and providing a function which takes care of the evolution of ξ in terms of the local equivalent strain e.

5 Numerical examples

The problem of spurious damage growth in the standard gradient-enhanced damage model has already been addressed by Geers et al. [8] with their STGD model. However, the STGD model is more computationally demanding than the standard one. In this section, one and two-dimensional examples are provided to demonstrate the merits of the proposed formulation in reproducing the same improvement at no extra computational cost compared to the CGD model. In both examples, quadratic and linear interpolation functions are used for the displacement and the nonlocal equivalent strain fields, respectively.

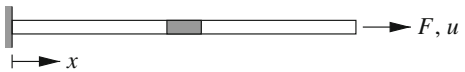

Fig. 1 Schematic configuration of the one-dimensional localization test. The shaded part indicates the imperfection (see Table 1 for geometry and constitutive model parameters)

As for the gradient activity parameter, the following evolution law has been considered:

$$\xi(e) = \begin{cases} c_0 + (c - c_0)\left(\frac{e}{e_\xi}\right)^{n_\xi} & \text{if } e \le e_\xi \\ c & \text{if } e > e_\xi \end{cases}. \tag{44}$$

This law is identical to (5) when $c_0 = 0$. However, to avoid division by zero in the system of governing equations (39) and to retain a quantitative resemblance with (5), c_0 is set to an arbitrary positive value which should be chosen such that nonlocal interaction is prevented at the initial time step. Our experience indicates that when the gradient activity parameter is smaller than the square of the distance between any two integration points, non-local interaction is effectively prevented and the model behaves like a local damage model. It is therefore sufficient to set c_0 smaller than the square of the shortest distance between any two integration points for (44) and (5) to be equivalent. Furthermore, when the material is completely unloaded, i.e. when $e = 0$, non-local interaction is prevented because (44) yields $\xi = c_0$ thus turning the gradient enhanced damage model into a local damage model.

The application of inverse procedures [5,11–13] through fitting of series of experimental results enables a phys-

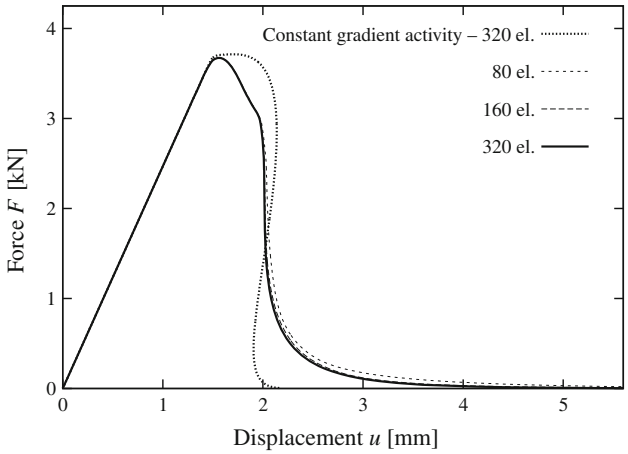

Fig. 2 Convergence of the force–displacement curve and comparison with the response of the CGD model in the one-dimensional localization test

ically-based determination of nonlocal and damage law parameters. Such techniques can be employed to calibrate c_0 in view of the equivalence between (5) and (44). To this end, it would be sufficient to determine c_0 with an inverse procedure such as that devised by Iacono et al. [11] on a series of synthetic data sets obtained with the original model by Geers et al. [8]. Other choices of c_0 can be physically motivated by the argument that initial material defects promote nonlocal interaction between material points [19].

5.1 One-dimensional localization test

The geometry and model parameters of the one-dimensional localization test borrowed from Geers et al. [8] are listed in Table 1. The bar, shown in Fig. 1, is loaded in tension and has a geometrical imperfection at the center. Conventional displacement control is used to compute the equilibrium path in the elastic regime, whereas a dissipation-based arc-length method [10] is employed thereupon so that any

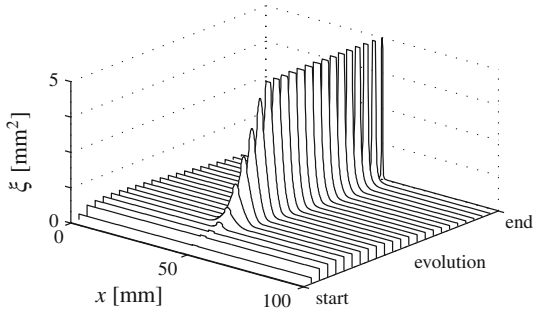

Fig. 4 Evolution of the gradient activity parameter in the one-dimensional localization test

possible snap-back is captured. The damage evolution law used in this example is the power law

$$\omega(\kappa) = 1 - \left(\frac{\kappa_\mathrm{i}}{\kappa}\right)^{\beta} \left(\frac{\kappa_\mathrm{c} - \kappa}{\kappa_\mathrm{c} - \kappa_\mathrm{i}}\right)^{\alpha}, \tag{45}$$

where the parameters α and β describe the rate of damage growth, and κ_i and κ_c are the initial and final equivalent strain values which correspond to $\omega = 0$ and $\omega = 1$, respectively. The local equivalent strain follows Mazars' definition according to which

$$e = \sqrt{\sum_{i=1}^{3} \langle \varepsilon_i \rangle_+}, \tag{46}$$

where $\langle \varepsilon_i \rangle_+$ are the positive principal strain components [14]. In Figs. 2, 3, 4, 5, and 6, the simulations were stopped as soon as $F < 0.001 F_\mathrm{max}$, where F_max is the maximum value reached by the reaction force F—this is denoted as complete loss of load-carrying capacity.

The results reported in Figs. 2, 3, 4, and 5 are identical to those reported by Geers et al. [8, Section 5.1]. The mesh objectivity of the model is clearly demonstrated by the force–displacement curves for three different discretizations shown in Fig. 2. For the sake of comparison, the force–displacement curve obtained with the CGD model is also reported.

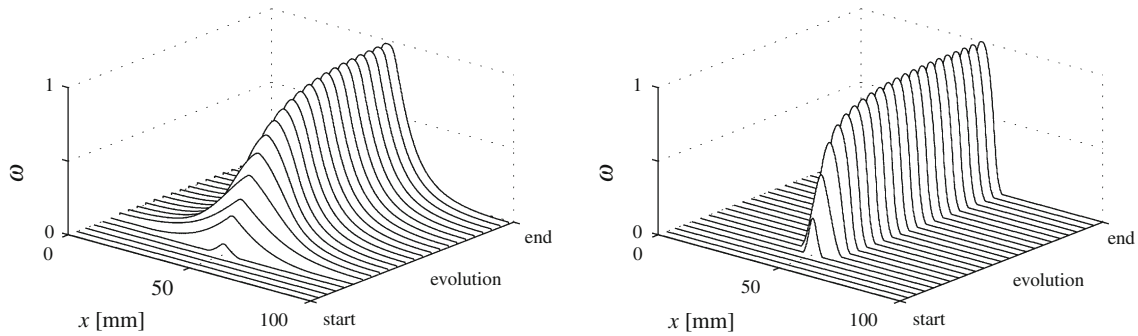

(a) Constant gradient activity **(b)** Transient gradient activity

Fig. 3 Damage evolution in the one-dimensional localization test. Note that here and in similar figures the end of the evolution process indicates complete loss of load-carrying capacity which occurs at different stages in the two models

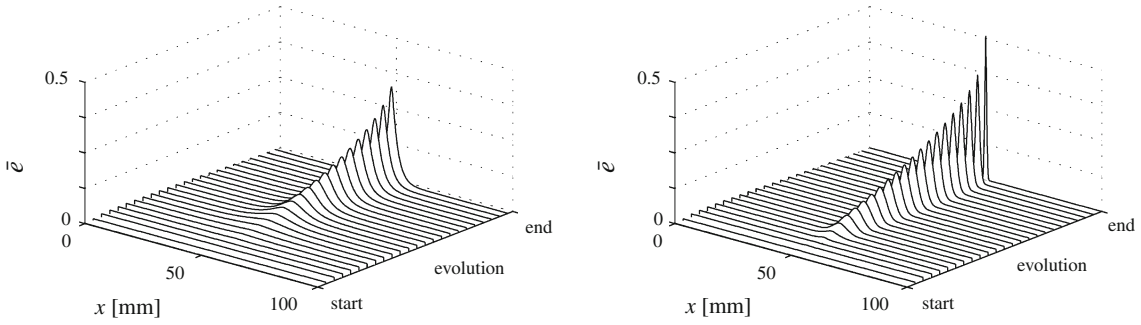

(a) Constant gradient activity **(b)** Transient gradient activity

Fig. 5 Nonlocal equivalent strain evolution in the one-dimensional localization test

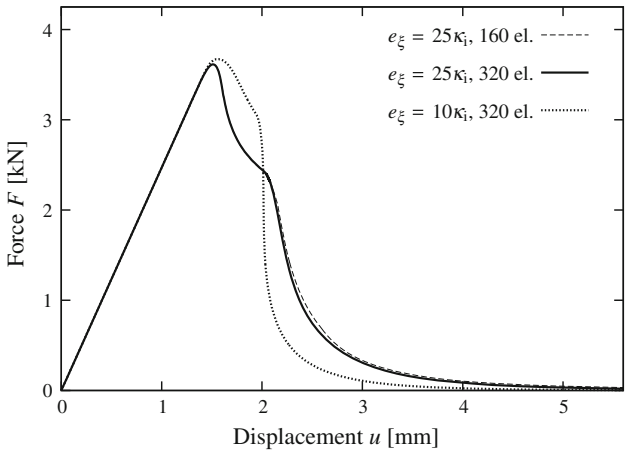

Fig. 6 Influence of the parameter e_ξ on the force–displacement curve in the one-dimensional localization test

Damage evolution is clearly influenced by the transient gradient activity parameter ξ. Indeed, the width of the damaged zone in Fig. 3b is narrower than that obtained with a constant gradient activity parameter shown in Fig. 3a. This is directly linked to the evolution of the gradient activity parameter ξ. As shown in Fig. 4, initial loading stages are characterized by an increase of the gradient activity along the whole bar with an evident strain localization in a finite zone. Within this region, the behavior of the model resembles that of the CGD model, while very small gradient interaction is present elsewhere. As the loading continues, the localization zone shrinks and the corresponding strain level increases, whereas the neighboring points around the process zone unload and the gradientactivity vanishes therein. As a result, the nonlocal interaction is confined to a finite region and the remaining parts of the bar behave in a strictly local manner. The equivalent strain in the fracture zone is no longer mapped to the surrounding material through nonlocal coupling and the damage profile does not widen.

An analogous comparison can be made between the nonlocal equivalent strain evolution of the two models reported in Fig. 5. With reference to the situation when the load-carrying capacity of the bar has been almost exhausted, i.e. at the end of the evolution process, the STGD model leads to a more localized response and higher values of the nonlocal strain compared to those of the CGD model. Oscillations in the nonlocal equivalent strain might arise once the nonlocal equivalent strain localizes in a single element at high deformation levels. Such oscillations, not reported here, can be resolved with a technique proposed in [8].

Computational experiments show that the structural behavior in the one-dimensional example depends upon the choice of the critical local strain e_ξ. Hence, it is worth investigating the influence of this parameter on the model performance. To this end, e_ξ is increased from 10 to 25 and the force–displacement curves for the two cases are compared in Fig. 6. The curve for latter case is shown for two different mesh densities. It can be seen that the regularization quality of the method is not influenced but the structural behaviors are significantly different. Therefore, the choice of this parameter does not affect the model performance but it should be calibrated for practical problems.

Another issue to address is the the effect of the damage evolution law on the model performance. To investigate the matter, the exponential damage evolution law

$$\omega = 1 - \frac{\kappa_i}{\kappa}\left[1 - \alpha + \alpha e^{-\beta(\kappa-\kappa_i)}\right] \tag{47}$$

with $\alpha = 0.99$, $\beta = 50$ and $\kappa_i = 0.005$ has been employed. Note that a power damage evolution law has been used in the previous numerical examples. As shown in Fig. 7a, the localization band starts widening at high deformation levels. This can be attributed to the shape of the softening law which is almost horizontal, i.e. characterized by a rate of change in the damage variable tending to zero, at high deformation levels. Numerical experiments indicate that the presence of a small residual stiffness in highly localized regions results in load redistribution to the neighboring points and hence reactivates the nonlocal averaging therein. To corroborate this claim, the same example is recomputed using the power softening

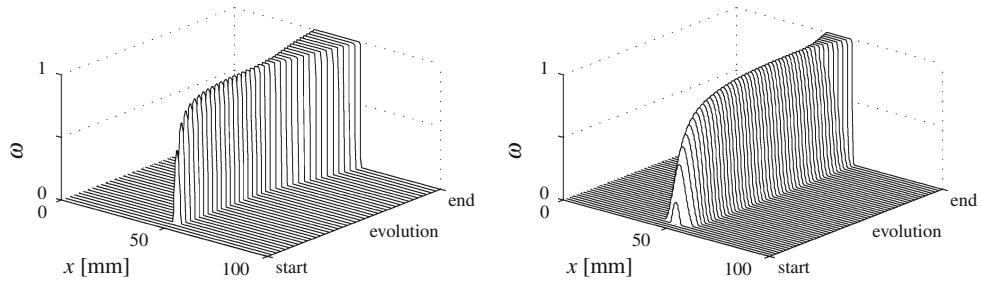

(a) Exponential evolution law **(b)** Modified power evolution law

Fig. 7 Damage evolution in the one-dimensional localization test with different damage evolution laws

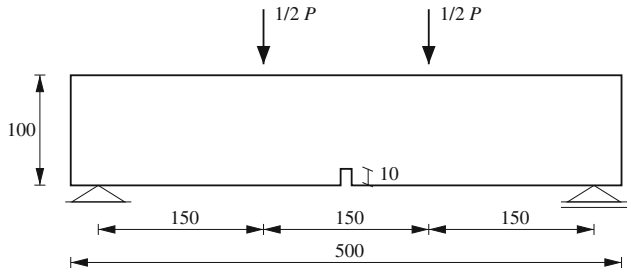

Fig. 8 Geometry and boundary conditions for the four-point bending test. All dimensions are in mm and thickness = 50 mm

law (45) in which an almost horizontal branch with the same residual stiffness as that of the exponential damage law is added at $\kappa = 0.7\kappa_c$. It can be observed in Fig. 7b that the same type of widening occurs at the very end of the simulation. This implies that the performance of the model at high deformation levels is highly sensitive to the choice of the damage evolution law. Nevertheless, this problem is particularly relevant when exponential damage laws are used because in such cases complete failure is never reached ($\omega \to 1$ for $\kappa \to \infty$) and thereby there exists a certain deformation level beyond which the rate of change in the damage variable tends to zero.

5.2 Concrete beam in four-point bending

To evaluate the model performance in two-dimensions, the four-point bending test of the concrete beam shown in Fig. 8 is considered. This problem has been previously analyzed by Pamin and de Borst [16] with a CGD model and by Simone et al. [20] with a continuous-discontinuous approach. Model parameters are listed in Table 2 and the beam is considered under plane stress conditions. Damage evolution follows an exponential damage law according to (47). The local equivalent strain is expressed by the modified von Mises definition according to which

$$e = \frac{k-1}{2k(1-2\nu)} I_1 + \frac{1}{2k}\sqrt{\frac{(k-1)^2}{(1-2\nu)} I_1^2 - \frac{12k}{(1+\nu)^2} J_2}, \quad (48)$$

where I_1 and J_2 are the first invariant of the strain tensor and the second invariant of the deviatoric strain tensor, respectively, k is the ratio of the compressive to tensile strength of concrete, and ν is the Poisson's ratio. Three different mesh sizes have been adopted in the simulations with element size h in the central part of the beam equal to 5, 2.5, and 1.25 mm for the coarse, medium and fine mesh, respectively. The medium mesh has been used for the results depicted in Figs. 9b, 10, 11, and 12.

The resulting load-deflection curves, reported in Fig. 9a, clearly indicate convergence to a unique solution upon mesh refinement. In these curves, the vertical displacement u of a point placed at the bottom and with an offset of 7.5 mm from the centerline of the beam has been used for the measurements of the deflection. Interestingly, as reported in Fig. 9b, there is almost no difference between the force–displacement curves obtained with the constant and transient gradient activity models. Damage evolution is however influenced by the choice of the model as shown in Fig. 10 and is explained further in the following.

The evolution of the damage field obtained with the CGD model is shown in the top row of Fig. 10. Damage widens significantly close to the notch as the deformation level increases. This eventually results in an unrealistically large damage profile close to failure which is a known feature of nonlocal and gradient-enhanced damage models with constant gradient activity and has been described in detail by Geers et al. [8] and Simone et al. [20].

The evolution of the damage field obtained with the transient gradient activity model is shown in the bottom row of Fig. 10. A careful examination of these profiles reveals that the widening issue, although less pronounced, is still present in the notch area. Similar to the one-dimensional example, the residual stiffness in the process zone results in the redistribution of the load to the neighboring points and hence increases the gradient activity parameter therein. This can be seen in Fig. 11. Reactivation of the nonlocal activity around the process zone leads high values of the nonlocal equivalent strain to be mapped from the process zone to the neighboring points and thereby yielding to widening of the damage pro-

Table 2 Parameters for the two-dimensional test

Model parameters	Quantity	Value	Units
Elastic parameters	Young's modulus E	40000	MPa
	Poisson's ratio ν	0.2	–
Nonlocal parameters	Gradient parameter c	4	mm^2
	n_ξ	1	–
	e_ξ	0.00075 ($=10\kappa_i$)	–
	c_0	0.01	–
von Mises local equivalent strain	k	10	–
Damage law	κ_i	0.000075	–
	α	0.92	–
	β	300	–

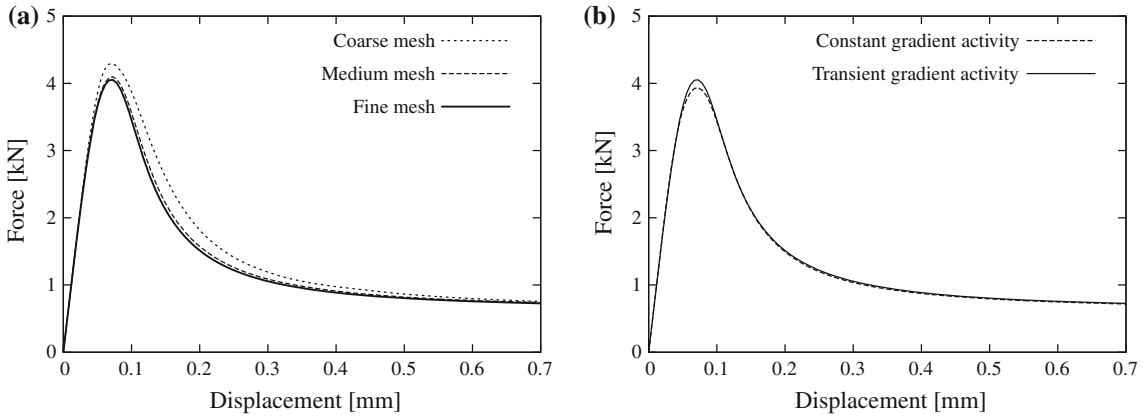

Fig. 9 Convergence of the force–displacement curve in the four-point bending test (**a**), and comparison of the force–displacement curve obtained with transient and constant gradient models (**b**)

file. This claim can be corroborated by a numerical example in which the damage evolution law is adjusted such that the energy dissipation rate is increased at intermediate deformation levels thus resulting in a very low residual stiffness. To this end, α in (47) is changed from 0.92 to 0.999. As evident from Fig. 13, the widening problem close to the notch is significantly alleviated. Despite this, the gradient activity parameter shown in Fig. 14 has a behavior similar to that reported in Fig. 11. This indicates that widening has only been postponed and will eventually occur with further loading as the dissipation rate in the softening law decreases.

6 Summary and final remarks

The original version of the gradient-enhanced damage model, equipped with constant gradient activity, suffers from spurious damage growth at final stages of failure. This spurred the development of a model with a transient internal length scale which successfully addresses this issue by employing an extra continuity equation.

In this contribution, a new formulation of the strain-based transient-gradient damage model is presented whereby a simple modification of the governing equations results in the elimination of the extra set of degrees of freedom required by the discretization of the extra continuity equation. The gradient activity parameter is associated to the local strain and it is thus mobilized in the process zone and neutralized elsewhere. This allows the model to appropriately describe the discontinuous nature of the displacement field at final stages of failure. Hence, the problem ofspurious damage growth in the constant gradient-enhanced damage model is eliminated. The merits of the method are demonstrated by means of one- and two-dimensional examples. It is shown that the presented method reproduces the same results as the original transient method while adopting a simpler and less computationally expensive formulation.

Finally, the influence of the choice of the critical local strain and the damage evolution law over the model performance have been investigated. With regard to the value of the critical local strain, it is observed that the regularization properties of the method are insensitive to this parameter but

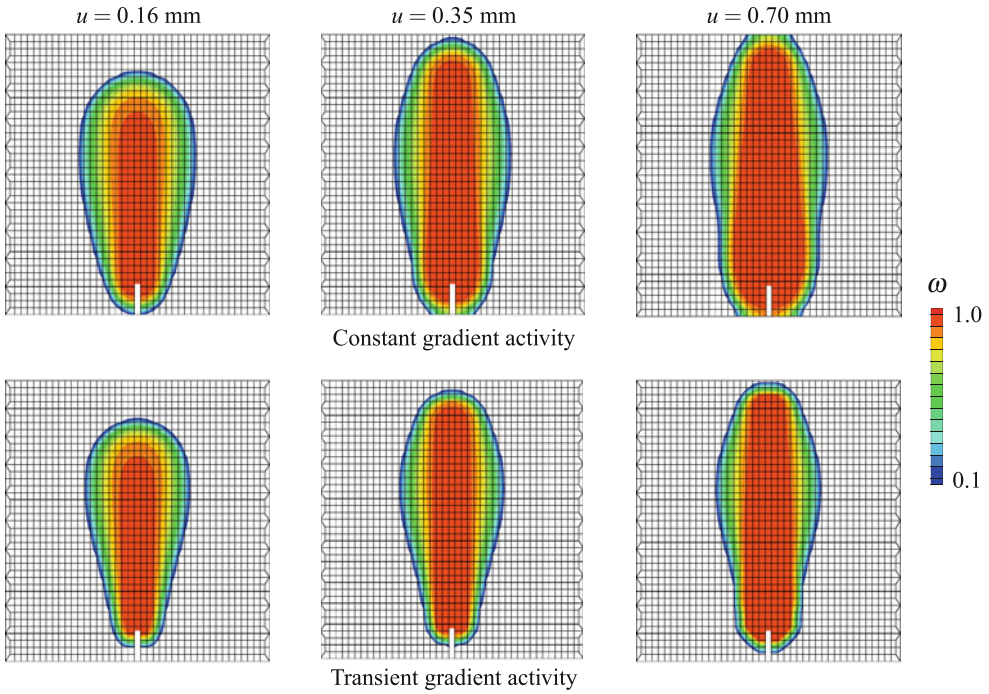

Fig. 10 Damage evolution for the constant and transient models in the four-point bending test

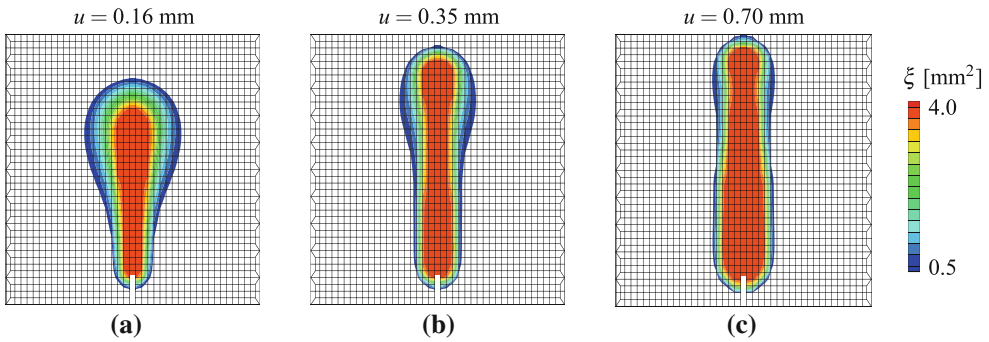

Fig. 11 Evolution of the gradient activity parameter in the four-point bending test

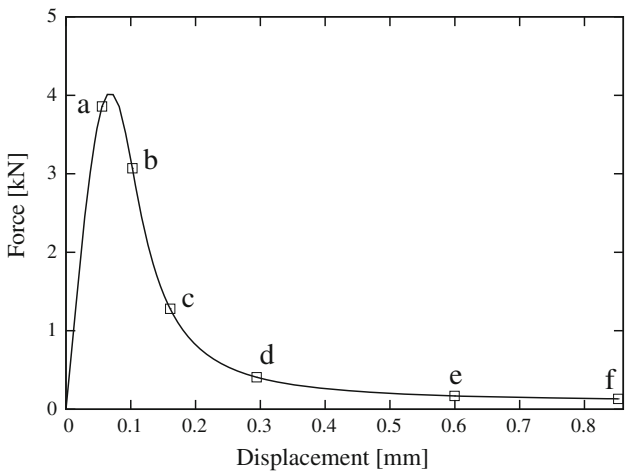

Fig. 12 Force–displacement curve in the four-point bending test with $\alpha = 0.999$

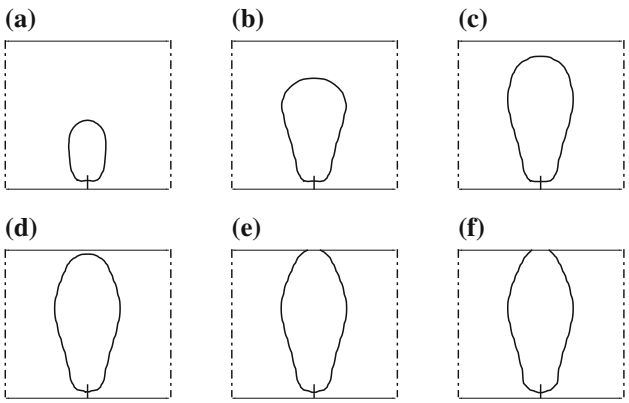

Fig. 13 Evolution of the damaged zone in the four-point bending test with $\alpha = 0.999$. Snapshots are taken at the points indicated in Fig. 12. On the contour line $\omega = 0.1$

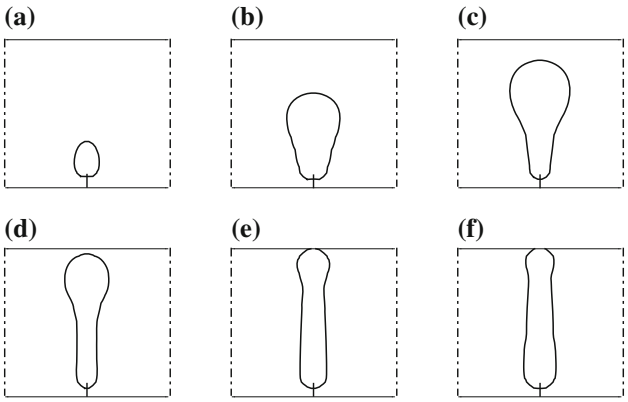

Fig. 14 Evolution of the gradient activity parameter in the four-point bending test with $\alpha = 0.999$. Snapshots are taken at the points indicated in Fig. 12. On the contour line $\xi = 0.5$ mm^2

the overall structural behavior is drastically influenced—this observation indicates the need for parameter calibration in applications. On the other hand, the model performance at very high deformation levels proves to be contingent upon the choice of the damage evolution law. It is indeed shown that the damage profile widens when there exists some residual stiffness in the process zone at high deformation levels. This feature is particularly evident when exponential damage laws are employed. As a result, the use of exponential damage laws in the type of models presented in this contribution should be avoided as they inevitably yield unphysical behavior at high deformation levels.

References

1. Bažant ZP (1991) Why continuum damage is nonlocal: micromechanical arguments. J Eng Mech 117:1070–1087
2. Bažant ZP (1994) Nonlocal damage theory based on micromechanics of crack interaction. J Eng Mech 120(3):593–617
3. Bažant ZP, Jirásek M (2002) Nonlocal integral formulations of plasticity and damage: survey of progress. J Eng Mech 128(11):1119–1149
4. Benvenuti E, Borino G, Tralli A (2002) A thermodynamically consistent nonlocal formulation for damaging materials. Eur J Mech A/Solids 21(4):535–553
5. Carmeliet J (1999) Optimal estimation of gradient damage parameters from localization phenomena in quasi-brittle materials. Mech Cohesive-Frict Mater 4(1):1–16
6. Desmorat R, Gatuingt F (2007) Introduction of an internal time in nonlocal integral theories. Internal report LMT 268, LMT-Cachan, URL http://hal.archives-ouvertes.fr/hal-00200898/en/
7. Desmorat R, Gatuingt F (2010) Introduction of an internal time in nonlocal integral theories. In: Bićanić N, Borst R, Mang HA, Meschke G (eds) Computational modelling of concrete structures—EURO-C 2010. Taylor & Francis Group, London, Rohrmoos/Schladming, Austria, pp 121–128
8. Geers MGD, de Borst R, Brekelmans WAM, Peerlings RHJ (1998) Strain-based transient-gradient damage model for failure analyses. Comput Methods Appl Mech Eng 160(1–2):133–153
9. Giry C, Dufour F, Mazars J (2011) Stress-based nonlocal damage model. Int J Solids Struct 48(25–26):3431–3443
10. Gutiérrez MA (2004) Energy release control for numerical simulations of failure in quasi-brittle solids. Commun Numer Methods Eng 20:19–29
11. Iacono C, Sluys LJ, van Mier JGM (2006) Estimation of model parameters in nonlocal damage theories by inverse analysis techniques. Comput Methods Appl Mech Eng 195(52):7211–7222
12. Le Bellégo C, Dubé JF, Pijaudier-Cabot G, Gérard B (2003) Calibration of nonlocal damage model from size effect tests. Eur J Mech A/Solids 22(1):33–46
13. Mahnken R, Kuhl E (1999) Parameter identification of gradient enhanced damage models with the finite element method. Eur J Mech A/Solids 18:819–835
14. Mazars J (1986) A description of micro- and macro-scale damage of concrete structures. Eng Fract Mech 25(5–6):729–737
15. Nguyen GD (2011) A damage model with evolving nonlocal interactions. Int J Solids Struct 48(10):1544–1559
16. Pamin J, de Borst R (1999) Gradient-enhanced damage and plasticity models for plain and reinforced concrete. In: Wunderlich W (ed) Proceedings of the European conference on computational mechanics—ECCM'99, Technical University of Munich, Munich, pp 482–483, paper no. 636
17. Peerlings RHJ, de Borst R, Brekelmans WAM, de Vree JHP (1996) Gradient-enhanced damage for quasi-brittle materials. Int J Numer Methods Eng 39(19):3391–3403
18. Pijaudier-Cabot G, Bažant ZP (1987) Nonlocal damage theory. J Eng Mech 113:1512–1533
19. Pijaudier-Cabot G, Haidar K, Dubé JF (2004) Non-local damage model with evolving internal length. Int J Numer Anal Methods Geomech 28(7-8):633–652
20. Simone A, Wells GN, Sluys LJ (2003) From continuous to discontinuous failure in a gradient-enhanced continuum damage model. Comput Methods Appl Mech Eng 192(41–42):4581–4607
21. Simone A, Askes H, Sluys LJ (2004) Incorrect initiation and propagation of failure in non-local and gradient-enhanced media. Int J Solids Struct 41(2):351–363
22. Voyiadjis GZ, Abu Al-Rub RK (2005) Gradient plasticity theory with a variable length scale parameter. Int J Solids Struct 42(14):3998–4029